Published in final edited form as:
J Mol Biol. 2009 April 17; 387(5): 1298–1308. doi:10.1016/j.jmb.2009.02.045.

Crystal Structures of Wild-type and Mutant Methicillin-resistant *Staphylococcus aureus* Dihydrofolate Reductase Reveal an Alternative Conformation of NADPH that may be Linked to Trimethoprim Resistance

Kathleen M. Frey, **Jieying Liu**, **Michael N. Lombardo**, **David B. Bolstad**, **Dennis L. Wright**, and **Amy C. Anderson***
Dept. of Pharmaceutical Sciences, University of Connecticut, 69 N. Eagleville Rd., Storrs, CT 06269

SUMMARY

Both hospital- and community-acquired *Staphylococcus aureus* infections have become major health concerns in terms of morbidity, suffering and cost. Trimethoprim-sulfamethoxazole (TMP-SMZ) is an alternative treatment for methicillin-resistant *S. aureus* (MRSA) infections. However, TMP-resistant strains have arisen with point mutations in dihydrofolate reductase (DHFR), the target for TMP. A single point mutation, F98Y, has been shown biochemically to confer the majority of this resistance to TMP. Using a structure-based approach, we have designed a series of novel propargyl-linked DHFR inhibitors that are active against several trimethoprim-resistant enzymes. We screened this series against wild-type and mutant (F98Y) *S. aureus* DHFR and found that several are active against both enzymes and specifically that the *meta*-biphenyl class of these inhibitors is the most potent. In order to understand the structural basis of this potency, we determined eight high-resolution crystal structures: four each of the wild-type and mutant DHFR enzymes bound to various propargyl-linked DHFR inhibitors. In addition to explaining the structure-activity relationships, several of the structures reveal a novel conformation for the cofactor, NADPH. In this new conformation that is predominantly associated with the mutant enzyme, the nicotinamide ring is displaced from its conserved location and three water molecules complete a network of hydrogen bonds between the nicotinamide ring and the protein. In this new position, NADPH has reduced interactions with the inhibitor. An equilibrium between the two conformations of NADPH, implied by their occupancies in the eight crystal structures, is influenced both by the ligand and the F98Y mutation. The mutation induced equilibrium between two NADPH binding conformations may contribute to decrease TMP binding and thus may be responsible for TMP resistance.

Keywords

MRSA; DHFR; *S. aureus*; TMP resistance; structure-based drug design

*Corresponding author: Mailing address: Dept of Pharmaceutical Sciences, University of Connecticut, 69 N. Eagleville Rd., Storrs, CT 06269. Phone: (860)486-6145. Fax: (860)486-6857. amy.anderson@uconn.edu.

Accession numbers Coordinates and structure factors have been deposited with the Protein Databank with accession numbers **3FQC**, **3FQ0**, **3F0B**, **3FQZ**, **3FQE**, **3FQO**, **3F0U** and **3FQV.**

INTRODUCTION

Staphylococcus aureus is a major cause of hospital-acquired infections. The increasing frequency of infections caused by methicillin-resistant *S. aureus* (MRSA) is of particular concern, especially in the United States where the prevalence is more than 55% in the intensive care unit[1]. MRSA has also become an established community-acquired infection among patients without established risk factors[2; 3]. Vancomycin is the preferred treatment for MRSA infections. However, vancomycin-intermediate *S. aureus* isolates (VISA) demonstrating a decreased sensitivity to the drug and vancomycin-resistant *S. aureus* (VRSA) strains have been reported in the US[4;5]. However, many strains of *S. aureus*, including new strains of community-acquired MRSA, show sensitivity to trimethoprim-sulfamethoxazole (TMP-SMZ). TMP is an antifolate that inhibits the essential enzyme, dihydrofolate reductase (DHFR) and SMZ inhibits dihydropteroate synthase.

Surveys from a collection of strains show that 28 % of MRSA isolates are TMP-resistant[6]. Examination of clinical isolates of TMP-resistant *S. aureus* reveals that intermediate resistance to TMP (MIC values ≤ 256 mg/L) is the most prevalent and is caused by three chromosomal mutations (H30N, F98Y and H149R) that occur in combinations as H30N/F98Y and F98Y/H149R. High-level TMP resistance (MIC values ≥ 512 mg/L) is conferred by a plasmid-encoded DHFR, called S1 DHFR[7] that contains three mutations (V31I, G43A, F98Y) relative to the sequence of DHFR from *S. epidermis*. Biochemical studies show that the single F98Y mutation in *S. aureus* DHFR (SaDHFR) and S1 DHFR is responsible for the most significant loss in TMP affinity[6;7]. The similarity of the k_{cat}/K_M values for the wild-type and Sa(F98Y) enzymes (3.12 vs. 2.36, respectively) suggests that the mutant enzyme capably catalyzes the reduction of folate, as expected.

Analysis of the crystal structures of the wild type and F98Y mutant SaDHFR bound to trimethoprim and folate, respectively[6] suggested that Tyr 98 forms a hydrogen bond with the backbone of Leu 5, thus preventing Leu 5 from forming a hydrogen bond with the 4-amino group on the pyrimidine ring of TMP. Unfortunately, the analysis is complicated by the fact that the mutant SaDHFR enzyme was crystallized with folate, which has a hydrogen bond acceptor at this position and not with a compound containing a hydrogen bond donor.

Iclaprim is a recently developed dihydrofolate reductase inhibitor that was designed to compensate for a loss of interactions between the mutant enzyme and TMP and form additional hydrophobic interactions with the active site pocket[8]. One of the suggestions of the inventors is that Iclaprim should be active against TMP-resistant MRSA, based on its additional interactions with the mutant enzyme. However, enzyme inhibition data from the Iclaprim patent (US patent 5,773,446) show that the compound still loses significant activity against the mutant enzyme (IC_{50} = 0.005 μM for the wild type and IC_{50} = 0.52 μM for the mutant). Furthermore, Iclaprim is only 4-fold more potent (IC_{50} = 0.52 μM) against the resistant enzyme than TMP (IC_{50} = 2.2 μM).

Using a structure-based approach, we previously developed a novel series of DHFR inhibitors with a propargyl-linked scaffold that is active against a number of trimethoprim-resistant enzymes[9; 10; 11]. In order to find a new class of antifolates effective against both the wild-type and trimethoprim-resistant forms of SaDHFR, we screened this group of compounds against both enzymes. We found that compounds falling into the *meta*-biphenyl subclass are potent inhibitors of both the wild-type and Sa(F98Y) mutant enzymes. High resolution crystal structures of the wild-type and Sa(F98Y)DHFR mutants bound to four propargyl-linked compounds reveal the basis of the increased potency of the *meta*-biphenyl class. In addition, with these structures we have discovered a new conformation of NADPH that predominantly exists in the mutant enzyme. The occupancy of this alternative conformation and the reduced

number of interactions it has with the inhibitors suggests that it may be an important contributor to the resistance mechanism of the F98Y mutation.

RESULTS

Resistance mutations have lowered the utility of trimethoprim as a clinically relevant therapeutic for MRSA infections. In previous work, we have described a class of novel DHFR inhibitors that is intended to inhibit DHFR enzymes that are natively trimethoprim-resistant such as *Bacillus anthracis*[9], *Candida glabrata*[11] and *Cryptosporidium hominis*[10]. This class of novel DHFR inhibitors is based on the trimethoprim scaffold but includes an extended propargyl linker between the 2,4-diaminopyrimidine and substituted phenyl rings (compounds **1**–**9** shown in Table 1). The purpose of the extended linker is to force the substituted phenyl ring deeper into a hydrophobic pocket in the active site, thereby increasing hydrophobic interactions. In addition to the propargyl linker, a distinguishing feature of some of the compounds in the class is a biphenyl ring system, which is installed either *meta* (compounds **10**–**14**) or *para* (compounds **15**–**17**) relative to the propargylic linker on the proximal phenyl ring. The biphenyl ring system was designed to take advantage of a second hydrophobic pocket near the proximal phenyl ring. These biphenyl compounds have proven to be very potent against DHFR from several different species including *C. hominis*[10] and *C. glabrata*[11].

Since there is evidence that the F98Y mutation reduces the interactions between the protein and ligand[6], we investigated whether the propargyl-based DHFR inhibitors, with an increased number of interactions, could function as potent inhibitors of both the wild-type and resistant enzymes. We tested an initial series of these compounds in enzyme assays with wild-type SaDHFR, a mutant (F98Y) trimethoprim-resistant SaDHFR and human DHFR to gauge selectivity (Table 1).

Our results confirm that while trimethoprim is an effective inhibitor for wild-type SaDHFR, its potency against the F98Y mutant decreases by 74-fold. In general, while the propargyl-based compounds are somewhat less potent against the wild-type enzyme than trimethoprim, several exhibit IC_{50} values in the low nanomolar range (specifically **5** and **8** – **13**). Importantly for all of these compounds, the fold-loss in potency between mutant and wild-type SaDHFR is significantly lower than the fold-loss of trimethoprim in the Sa(F98Y) mutant. Specifically, compounds **10**–**14**, the *meta*-biphenyl series, are potent compounds that lose less than 5-fold potency in the resistant mutant. While selectivity against the human enzyme has not yet been optimized, the *meta*-biphenyl compounds already show the greatest degrees of selectivity at the enzyme level.

Structures of the wild-type and mutant enzymes bound to DHFR inhibitors

In order to begin to optimize potency and selectivity for these compounds against both the wild-type and resistant mutant, we obtained four pairs of crystal structures: Sa and Sa(F98Y) DHFR bound to cofactor NADPH and ligands **5**, **8**, **10**, and **15** (one from each class in Table 1). Seven of the eight crystals share the same unit cell dimensions and $P6_122$ space group as the Sa(F98Y)-folate structure, therefore these structures were solved using difference Fourier methods using the Sa(F98Y)-folate structure as a model[6] (Table 2). The crystals for the SaDHFR:NADPH:**5** complex belong to space group $P6_1$; this structure was determined by molecular replacement with two molecules in the asymmetric unit. With the high-resolution data that were collected for the majority of the ternary complexes, electron density for each complex was well resolved throughout the structure (see Fig. 2 for an example), allowing the positions of the ligand, cofactor and amino acids to be refined to have excellent agreement with the diffraction data (Table 2).

The overall structures have the characteristic "DHFR fold," featuring an eight-stranded β sheet and four alpha helices connected by flexible loops. The conformations of the Sa(F98Y)-folate structure[6] and the Sa(F98Y)-ligand complexes reported here are similar with root-mean square deviations between 157 Cα atoms of 0.3 Å. –

The resolution of the structures allowed a thorough examination of interactions between the ligands and the active site residues (Fig. 1a–d). In all structures, the conserved acidic residue Asp 27 forms two hydrogen bonds with the protonated N1 atom and the 2-amino group of the diaminopyrimidine ring. The 4-amino group forms two additional hydrogen bonds with the backbone carbonyl oxygen atoms of residues Leu 5 and Phe 92. The C6 methyl or ethyl groups form van der Waals interactions with residues Leu 20 and Leu 28. Phe 92 is within 3.8 Å of the propargyl linker, suggesting a possible π- π stacking interaction.

The structural analysis clarifies the basis of the increased potency of the *meta*-biphenyl compounds. While the proximal substituted phenyl rings (relative to the pyrimidine ring) form roughly equivalent interactions with residues Ile 50 and Phe 92, the distal *meta*-biphenyl ring extends deeper into the pocket and increases contacts with these hydrophobic residues as well as with Leu 54 and Leu 28. We hypothesize that substitutions on the distal phenyl ring would further increase interactions. For example, hydrophobic interactions may be formed between the 2,6-dimethyl groups on compound **12** and residues Val 31 and Leu 54. Structures of the *para*-biphenyl compounds (for example, compound **15**) reflect that the biphenyl group is projected out of the active site pocket in both conformations, decreasing binding and resulting in higher IC_{50} values.

The crystal structure of the complex of the wild-type enzyme with **10** revealed two distinct ligand conformations for this compound (Fig. 1c). Compound **10** adopts a similar conformation as observed in the Sa(F98Y) structure with 80 % occupancy. The second conformation has 20 % occupancy and varies in the positioning of the biphenyl.

The conformations of NADPH and the effect of the F98Y mutation

Earlier work with SaDHFR and Sa(F98Y)DHFR suggested that the mechanism of resistance to trimethoprim is mediated by the loss of a key hydrogen bond between the 4-amino group on the pyrimidine and the carbonyl oxygen of Leu 5[6;8]. The authors propose that Tyr 98 forms a new hydrogen bond with the carbonyl oxygen of Leu 5, thus preventing the formation of the aforementioned hydrogen bond. Chemical shifts of ^{15}N-labeled trimethoprim in the presence of the wild-type and mutant enzymes reflect the absence of the hydrogen bond between the 4-amino group on trimethoprim and the mutant enzyme. However, the structures reported here and the published structure of iclaprim bound to Sa(F98Y)DHFR[8], reveal that both the 4-amino group and the Tyr 98 hydroxyl are capable of forming hydrogen bonds with the carbonyl oxygen of Leu 5. The strength of the hydrogen bonds in this bifurcated acceptor system (O-H•••O•••H-N) is undetermined relative to the single hydrogen bond (O•••H-N) found in the wild-type system. However, in studies using a model depsipeptide, the bifurcated system was shown to be enthalpically slightly favorable (1 kcal/mol) and entropically slightly unfavorable (3 eu), relative to the combination of the individual hydrogen bonds[12]. In a highly organized active site, it would be assumed that additional entropic penalties would be minimal. It also seems unlikely that the pyrimidine ring of trimethoprim would exhibit very different hydrogen bonding patterns than iclaprim or the ligands reported here. Given the fact that the stability of this hydrogen bonding network may range from slightly stabilizing to weakly destabilizing, it is unclear that this change is solely responsible for the observed drop in affinity for trimethoprim. Therefore, we sought a structural explanation for the loss of affinity observed with the propargyl-linked ligands and Sa(F98Y)DHFR.

During refinement of the structures reported here, we discovered a unique conformation of NADPH that may also contribute to an antifolate resistance mechanism. This alternative conformation is most prevalent in the structures of Sa(F98Y) bound to ligands **5** (Figures 1a and 3e) and **8** (Figures 1b and 3f). In the new conformation, the pyro-phosphate of NADPH is rotated and the ribose and nicotinamide ring are closer than in the standard extended conformation. For example, the distance between the 3′ ribose hydroxyl and the nicotinamide carbon is 2.77 Å and 3.62 Å in the alternative and standard extended conformations, respectively.

Minimizing the energy of the new NADPH conformation using Sybyl prevented steric interactions between the ribose hydroxyl and the proton associated with the neighboring carbon of the nicotinamide ring. The minimized conformation was then used in all further cycles of refinement. The clear density in the omit F_o-F_c map (Fig. 2) confirms the validity of the new alternative conformation. Reinforcing the validity of the new conformation, temperature factors for the ligands and cofactors are either at or below the average value for the entire complex.

Tyr 98 appears to influence an equilibrium between the bound conformations of the ligand, NADPH, and conserved residues involved in diaminopyrimidine binding. Since the conformation of NADPH fully switches from the standard extended form in the structure with SaDHFR:NADPH:**5** to the alternative form in the Sa(F98Y):NADPH:**5**, this structural pair best demonstrates the effect of the Tyr 98 mutation. The Tyr 98 mutation introduces a repulsive interaction between the Tyr hydroxyl group and the nicotinamide ring carbonyl. To overcome the repulsion, NADPH adopts the alternative conformation, allowing three water molecules to be coordinated between the Tyr 98 hydroxyl and the nicotinamide carbonyl (Figures 2, 3a and 3e). Electron density for these three water molecules is strongly evident in the F_o-F_c difference map at 3.5 sigma (Figure 2). As a result of the new conformation, NADPH does not form as many hydrophobic interactions with the ligand near the propargyl linker and Phe 92, an important factor that may contribute to the fold-loss exhibited in IC_{50} values between the wild-type and mutant proteins.

In the other structural pairs, there is varying occupancy of the standard and alternative conformations of NADPH (Table 3). In the Sa(F98Y) structure with compound **8**, both the extended and alternative conformations of NADPH are present with occupancies of 70 % and 30 %, respectively (Fig. 3b, 3f). When the alternative conformation of NADPH is present, it forms the same interactions as described above in the complex with SaDHFR(F98Y):NADPH:**5**. In complexes of both the wild-type and mutant SaDHFR with NADPH and compound **10**, the standard conformation of NADPH is present at 100 % occupancy and the water molecules associated with the alternative conformation are not present (Fig. 3c, 3g). Finally, both conformations of NADPH are present in the structures of SaDHFR and Sa(F98Y)DHFR bound to compound **15** (Fig. 3d, 3h). The wild-type SaDHFR structure presents a unique situation in which the alternative NADPH conformation exists at 70 % occupancy without the presence of the Tyr 98 hydroxyl. In this structure, a water molecule near Phe 98 in the wild-type structure forms a hydrogen bond to the carbonyl oxygen atoms of Phe 92 and the nicotinamide ring of both NADPH conformations. Interestingly, Phe 92 undergoes a conformational change, relative to other wild-type SaDHFR structures, in order to form this bond. Compound **15** is also present in two conformations that may stabilize the multiple conformations of NADPH. Perhaps correspondingly, the potency of **15** for the wild-type enzyme is also lower, with an IC_{50} value of 0.17 μM.

Like its corresponding wild-type structure, Sa(F98Y) DHFR bound to **15** has the alternative conformation of NADPH present at 70 % occupancy. Compound **15** is also present in multiple conformations, and similar to the wild-type structure, may stabilize the multiple conformations

of NADPH. The presence of the mutation affects the binding equilibrium, where another network of hydrogen bonds is formed between Tyr 98, Leu 5, a coordinated water molecule, and the nicotinamide ring of the new NADPH conformation. The presence of the alternative NADPH conformation in both Sa and Sa(F98Y) structures with **15** suggests that the chemical structure of the ligand can affect the overall equilibrium between the bound states within the ternary complex.

Overall, the eight structures suggest that there is a ligand-influenced equilibrium between the bound states of the protein, associated water molecules, NADPH and ligand. The chemical structures of the ligands may lend some insight into the interpretation of the NADPH conformations. Compound **5** has a *gem*-dimethyl substitution at the propargyl linker that may form hydrophobic interactions stabilizing the new NADPH conformation. On the other hand, structures with compound **8**, with an unsubstituted propargyl linker, show only 70 % occupancy of the alternative conformation. The *meta*-biphenyl of compound **10** increases the interactions with the hydrophobic pocket and uses these interactions to force the propargyl methyl group closer to the nicotinamide, thus stabilizing the extended conformation of NADPH in Sa(F98Y) DHFR. The *para*-biphenyl in compound **15** is found in two distinct conformations that can stabilize interactions with both conformations of NADPH.

Comparison with structures of human DHFR

Comparing the structures reported here with human DHFR, we see several opportunities to improve the selectivity of the lead compounds. Structural evidence and assay data agree that the *meta*-biphenyl series form several strong interactions and retain the greatest degree of selectivity over the human enzyme. Selectivity for these compounds can most likely be attributed to specific structural differences located on the helix closest to the diaminopyrimidine. In the human enzyme, this helix contains Phe 31 and Phe 34, while the SaDHFR enzymes have Leu 28 and Val 31 respectively, in these positions (Fig. 4). These bulkier residues in the human enzyme might sterically interfere with the *meta*-biphenyl ligands and reduce the overall potency. A bulkier substitution at the C6 position of the pyrimidine ring can also be explored to decrease potency and gain selectivity for the human enzyme. We speculate that the potency of compound **9** results from the *n*-propyl substitution at this C6 position. Another critical difference between the bacterial and human DHFR structures is the presence of a loop at the active site in human DHFR (Pro 61- Asn 64) that is absent in SaDHFR (Fig. 4). The *meta*-biphenyl series of compounds may introduce sterically demanding bulk near this loop in human DHFR that lowers affinity between the compounds and the enzyme.

DISCUSSION

The prevalence and impact of infections caused by *S. aureus* and specifically, MRSA, is increasing worldwide at an alarming rate. Especially concerning is the fact that the organism appears to be particularly adept at acquiring new mechanisms of resistance to accepted therapeutic strategies. The successful use of trimethoprim in combination with sulfamethoxazole, has validated the use of antifolates in combating this disease. However, TMP-resistant MRSA strains have now appeared in the US and strategies to develop new antifolates capable of inhibiting both wild-type and TMP-resistant strains are necessary.

We present, in this work, a group of novel antifolates that are characterized by a propargyl-linked pyrimidine and substituted biphenyl system. The best of these compounds inhibit the wild-type enzyme with IC_{50} values in the nanomolar range and lose only 2-4-fold potency when evaluated with the TMP-resistant F98Y enzyme. Crystal structures of the wild-type and Sa(F98Y) enzymes bound to four of these inhibitors reveal the structural basis of the potency measured in enzyme inhibition assays. The increased number of interactions with the

hydrophobic pocket comprised of Thr 46, Ile 50 and Leu 54, relative to trimethoprim, may partially explain the low loss of affinity observed with the mutant enzyme.

The crystal structures and enzyme inhibition data suggest designs for a second generation of compounds that have increased potency and selectivity. Specifically, the SAR study shows that an ethyl or *n*-propyl substitution at C6 yields increased potency and fits in the hydrophobic pocket near Leu 20, Leu 28 and Val 31. Since the initial series of biphenyl compounds contain only a methyl at this position, *meta*-biphenyl compounds with longer alkyl chains at C6 are planned for synthesis and evaluation. Likewise, the ethyl and *gem*-dimethyl substitutions at the propargylic position led to an increase in potency, possibly by forming contacts with Phe 92; these substitutions will be evaluated in the context of the *meta*-biphenyl class. Finally, the hydrophobic pocket that binds the distal aryl ring appears to be large enough to accommodate additional bulk, thus potentially leading to increased interactions. Interestingly, the alternate conformations of compound **10** in the crystal structure with Sa(F98Y)DHFR yield evidence of the volume of this pocket and the ability of the inhibitors to accumulate additional interactions. Since the structure of the human DHFR enzyme has specific residue substitutions and insertions relative to the SaDHFR structure, it is likely that longer alkyl chains at the C6 position and increased bulk in the distal biphenyl ring will yield increases in selectivity as well.

Not only is it possible to evaluate protein:ligand interactions with these eight structures, we observe a novel conformation of NADPH in several of the structures. The alternative conformation is primarily associated with the mutant enzyme since the introduction of the Tyr 98 hydroxyl promotes a hydrogen bonding network with three water molecules and the new conformation of the nicotinamide ring. The alternative conformation of NADPH exhibits drastically reduced hydrophobic interactions with the ligands, a factor that could easily explain some of the loss of affinity between these ligands and the Sa(F98Y)DHFR enzyme. Importantly, the structure of Sa(F98Y) DHFR with NADPH and folate retains the standard conformation of NADPH[6], explaining the catalytic competency of the mutant enzyme.

The ligand-dependent NADPH conformations observed in these structures suggest that trimethoprim, also, may affect the equilibrium of the bound states of the protein and NADPH in the ternary complex of the F98Y mutant. Earlier literature has suggested a cooperative binding relationship between trimethoprim and NADPH [13;14; 15]. If, in fact, potency is lost with the alternative NADPH conformation because of reduced interactions between the nicotinamide ring and the linker between the pyrimidine and phenyl rings, then the amplified fold-loss (74-fold for trimethoprim) may be explained by the shorter linker and the smaller group in the hydrophobic pocket.

The *meta*-biphenyl class of inhibitors is clearly the best lead for future efforts to develop a potent inhibitor of both the wild-type and mutant enzymes. Not only are these compounds the most potent and selective, they maintain interactions with the nicotinamide ring of NADPH by not inducing the altered conformation of the cofactor, even in the environment of the F98Y mutation. The standard extended conformation of NADPH, observed at full occupancy in the structure of the mutant enzyme, along with the additional interactions of the biphenyl, most likely contribute to the overall binding affinity and minimal fold-loss in potency for compound **10**.

MATERIALS AND METHODS

Cloning, Expression, and Purification

Genomic DNA for wild-type *S. aureus* was purchased from ATCC (#700699) and used as a template for PCR. Primers were designed to amplify the region encoding the DHFR gene. The insert was ligated into vector pET41 that contains an 8X-histidine tag for purification. A site-

directed mutagenesis experiment was used to change Phe 98 in the wild-type DHFR to Tyr 98. Final clones for SaDHFR and Sa(F98Y) DHFR were verified and analyzed by sequencing. We maintained the significant literature precedent for beginning the residue numbering of SaDHFR with Met 0.

Recombinant Sa and Sa(F98Y) DHFR were over expressed in *E. coli* BL21(DE3) cells and grown for an additional 6 hours at 30°C after induction with 1 mM IPTG. 1L cell pellets were lysed with 1X Bugbuster (Novagen) and DNase. Lysate was centrifuged for 20 minutes at 18,000 RPM and the soluble protein was extracted. DHFR enzyme was purified using nickel affinity chromatography. Both proteins were desalted into 20 mM Tris, 20 % glycerol, 0.1 mM EDTA, and 2 mM DTT (pH 8.0) using a PD-10 column (GE Healthcare). Protein was concentrated to ~5 mg/mL, aliquoted into 500 μL samples, and flash frozen with liquid nitrogen. All samples were stored at −80 °C.

Enzyme Inhibition Assays

Enzyme inhibition assays were performed by monitoring the rate of NADPH oxidation by the DHFR enzyme at an absorbance of 340 nm. Assays were performed in the presence of saturating concentrations of NADPH and initiated with dihydrofolate. All assays were completed at 25 °C in a buffer containing 20 mM TES pH 7.0, 50 mM KCl, 10 mM 2-mercaptoethanol, 0.5 mM EDTA and 1 mg/mL BSA. Inhibition was measured at least three times with inhibitor concentrations near the IC_{50} value and the average IC_{50} value is reported with a standard deviation [9;10; 11].

Crystallization

Sa and Sa(F98Y) DHFR were co-crystallized with **5**, **8**, and **10** and **15** using the hanging drop vaporization method. Protein (12 mg/mL) was incubated with ligand (1 mM) and NADPH (2 mM) for two hours on ice. An equal volume of the protein:ligand:NADPH complex was mixed with an optimized crystallization solution consisting of 15 % PEG 10,000, 150 mM sodium acetate, 100 mM MES pH 6.5, and 5 % butyrlactone (Sigma Aldrich). All crystal growth followed the same procedures and typically yielded crystals within 5–7 days. Crystals were incubated in a cryo-protectant buffer containing 15 % glycerol then flash-cooled with liquid nitrogen. High resolution data sets were collected at Brookhaven NSLS on beamline X29.

Structure Determination

Data were indexed and scaled used HKL2000[16]. Crystal structures for all complexes were solved using a model of Sa(F98Y) DHFR bound to folate [6]. The earlier model shares the same hexagonal space group ($P6_122$) and unit cell dimensions as seven of the currently described crystals, therefore difference Fourier methods were used to solve the phase problem for these data. The crystals of SaDHFR:NADPH:**5** belong to space group $P6_1$ and there are two molecules in the asymmetric unit. Therefore, this structure was determined by molecular replacement using Phaser[17]. The programs COOT [18] and Refmac5 19 were used to build and refine the structure until an acceptable R_{cryst} and R_{free} were achieved. Structure geometry was evaluated using Procheck [20] and Ramachandran plots.

Inhibitors

The synthesis and complete characterization of compounds **1**–**17** have been described previously [9;10; 11; 21; 22].

Acknowledgments

The authors thank the scientists at Hoffman-LaRoche & Co. for providing the coordinates of Sa(F98Y) DHFR bound to NADPH and folate. The authors thank Erin Bolstad for performing the energy calculations for NADPH and the NIH for providing funding (GM067542 and AI073375 to ACA and R41 AI065143 to DLW).

Abbreviations

MRSA
: methicillin-resistant *S. aureus*

VISA
: vancomycin-intermediate *S. aureus*

VRSA
: vancomycin-resistant *S. aureus*

TMP
: trimethoprim

SMZ
: sulfamethoxazole

MSSA
: methicillin-sensitive *S. aureus*

DHFR
: dihydrofolate reductase

MIC
: minimum inhibition concentration

Sa DHFR
: dihydrofolate reductase from *S. aureus*

SaDHFR (F98Y)
: dihydrofolate reductase from *S. aureus* with the F98Y mutation

IC_{50}
: inhibition concentration 50%

WT
: wild-type

NADPH
: nicotinamide adenine dinucleotide phosphate, reduced form

References

1. National Nosocomial Infections Surveillance (NNIS) System. National Nosocomial Infections Surveillance (NNIS) System Report, data summary from January 1992 through June 2004, issued October 2004. Am J Infect Control 2004;32:470–485. [PubMed: 15573054]
2. Kluytmans-VandenBergh M, Kluytmans J. Community-acquired methicillin-resistant *Staphylococcus aureus*: current perspectives. Clin Microbiol Infect 2006;12 (suppl 1):9–15. [PubMed: 16445719]
3. Kollof M, Micek S. Methicillin-resistant *Staphylococcus aureus*: a new community-acquired pathogen? Curr Opin Infect Dis 2006;19:161–168. [PubMed: 16514341]
4. Appelbaum P. MRSA- the tip of the iceberg. Clin Microbiol Infect 2006;12 (Suppl 2):3–10. [PubMed: 16524422]

5. Drew R. Emerging Options for treatment of invasive, multidrug-resistant *Staphylococcus aureus* infections. Pharmacotherapy 2007;27:227–249. [PubMed: 17253914]
6. Dale G, Broger C, D'Arcy A, Hartman P, DeHoogt R, Jolidon S, Kompis I, Labhardt A, Langen H, Locher H, Page M, Stuber D, Then R, Wipf B, Oefner C. A single amino acid substitution in Staphylococcus aureus dihydrofolate reductase determines trimethoprim resistance. J Mol Biol 1997;266:23–30. [PubMed: 9054967]
7. Dale G, Broger C, Hartman P, Langen H, Page M, Then R, Stuber D. Characterization of the gene for the chromosomal dihydrofolate reductase (DHFR) of *Staphylococcus epidermis* ATCC 14990: the origin of the trimethoprim-resistant S1 DHFR from *Staphylococcus aureus*? J Bacteriol 1995;177:2965–2970. [PubMed: 7768789]
8. Schneider P, Hawser S, Islam K. Iclaprim, a novel diaminopyrimidine with potent activity on trimethoprim sensitive and resistant bacteria. Bioorg Med Chem Lett 2003;13:4217–4221. [PubMed: 14623005]
9. Beierlein J, Frey K, Bolstad D, Pelphrey P, Joska T, Smith A, Priestley N, Wright D, Anderson A. Synthetic and crystallographic studies of a new inhibitor series targeting *Bacillus anthracis* dihydrofolate reductase. J Med Chem 2008;51:7532–7540. [PubMed: 19007108]
10. Bolstad D, Bolstad E, Frey K, Wright D, Anderson A. A structure-based approach to the development of potent and selective inhibitors of dihydrofolate reductase from *Cryptosporidium*. J Med Chem 2008;51:6839–6852. [PubMed: 18834108]
11. Liu J, Bolstad D, Smith A, Priestley N, Wright D, Anderson A. Structure-guided development of efficacious antifungal agents targeting *Candida glabrata* dihydrofolate reductase. Chem Biol 2008;15:990–996. [PubMed: 18804036]
12. Yang J, Christianson L, Gellman S. Comparison of an HXH Three-Center Hydrogen Bond with Alternative Two-Center Hydrogen Bonds in a Model System. Org Lett 1999;1:11–14.
13. Baccanari D, Kuyper L. Basis of selectivity of antibacterial diaminopyrimidines. J Chemother 1993;5:393–399. [PubMed: 8195830]
14. Birdsall B, Burgen A, Roberts G. Binding of coenzyme analogues to *Lactobacillus casei* dihydrofolate reductase: binary and ternary complexes. Biochemistry 1980;19:3723–3731. [PubMed: 6773548]
15. Kovalevskaya N, Smurnyy Y, Polshakov V, Birdsall B, Bradbury A, Frenkiel T, Feeney J. Solution structure of human dihydrofolate reductase in its complex with trimethoprim and NADPH. J Biomol NMR 2005;33:69–72. [PubMed: 16222560]
16. Otwinowski, Z.; Minor, W. Processing of X-ray diffraction data collected in oscillation mode. In: Carter, CW.; Sweet, RM., editors. Methods in Enzymology. Vol. 276. Academic Press; New York: 1997. p. 307-326.
17. McCoy A. Solving structures of protein complexes by molecular replacement with Phaser. Acta Cryst 2007;D63:32–41.
18. Emsley P, Cowtan K. Coot: Model-building tools for molecular graphics. Acta Cryst 2004;D60:2126–2132.
19. Murshudov G, Vagin A, Dodson E. Refinement of macromolecular structures by the maximum-likelihood method. Acta Cryst 1997;D53:240–255.
20. Laskowski R, MacArthur M, Moss D, Thornton J. PROCHECK: a program to check the stereochemical quality of protein structures. J Appl Cryst 1993;26:283–291.
21. Pelphrey P, Popov V, Joska T, Beierlein J, Bolstad E, Fillingham Y, Wright D, Anderson A. Highly efficient ligands for DHFR from *Cryptosporidium hominis* and *Toxoplasma gondii* inspired by structural analysis. J Med Chem 2007;50:940–950. [PubMed: 17269758]
22. Liu J, Bolstad D, Smith A, Priestley N, Wright D, Anderson A. Probing the active site of *Candida glabrata* dihydrofolate reductase with high resolution crystal structures and the synthesis of new inhibitors. Chem Biol Drug Des 2008;73:62–74. [PubMed: 19152636]

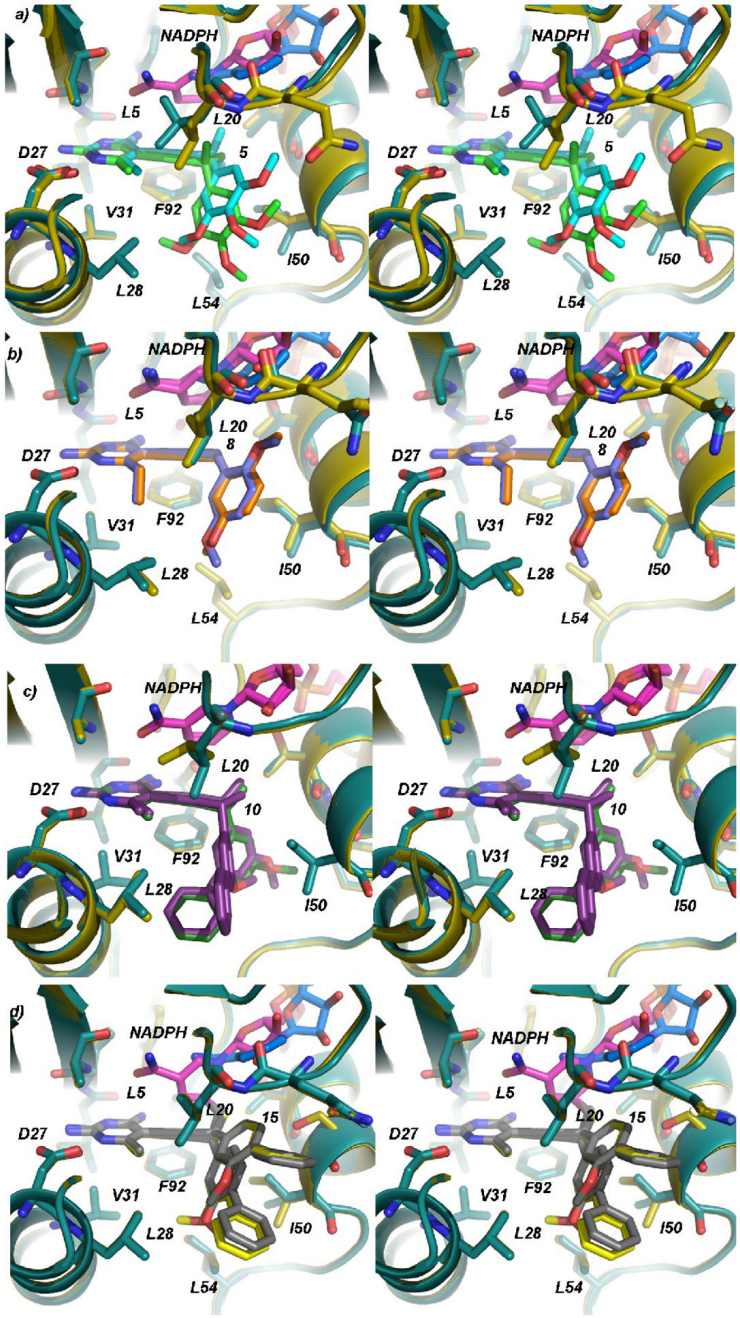

Figure 1.

Stereoview images of the wild-type (teal) and Sa(F98Y) mutant (gold) enzymes bound to a) compound **5** (wild-type light green, F98Y cyan), b) compound **8** (wild-type orange, F98Y lavender), c) compound **10** (wild-type purple, F98Y dark green) and d) compound **15** (wild-type yellow, F98Y gray). The standard conformation of NADPH is shown in magenta and the alternative conformation is shown in blue. Water molecules (shown in Figure 3) are omitted here for clarity.

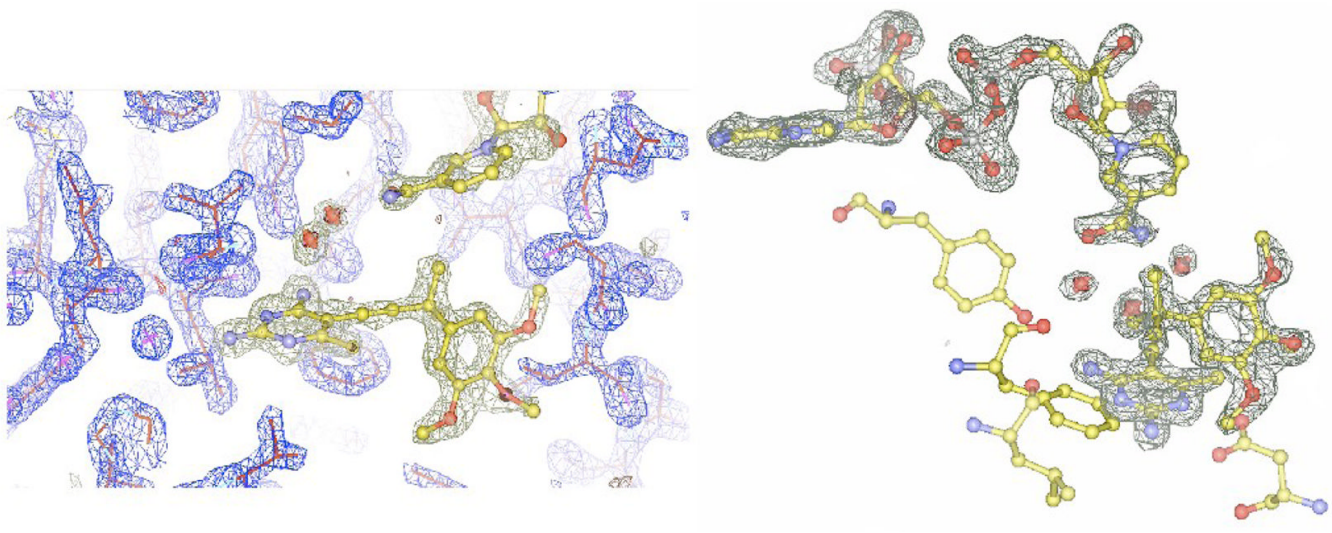

Figure 2.
Electron density at the active site for SaDHFR(F98Y):NADPH:**5**. Protein is shown with $2F_o$-F_c density (1.5 σ, blue) and ligands are shown with omit F_o-F_c density (3.0 σ, grey). A full view of the density for the alternative conformation is shown on the right.

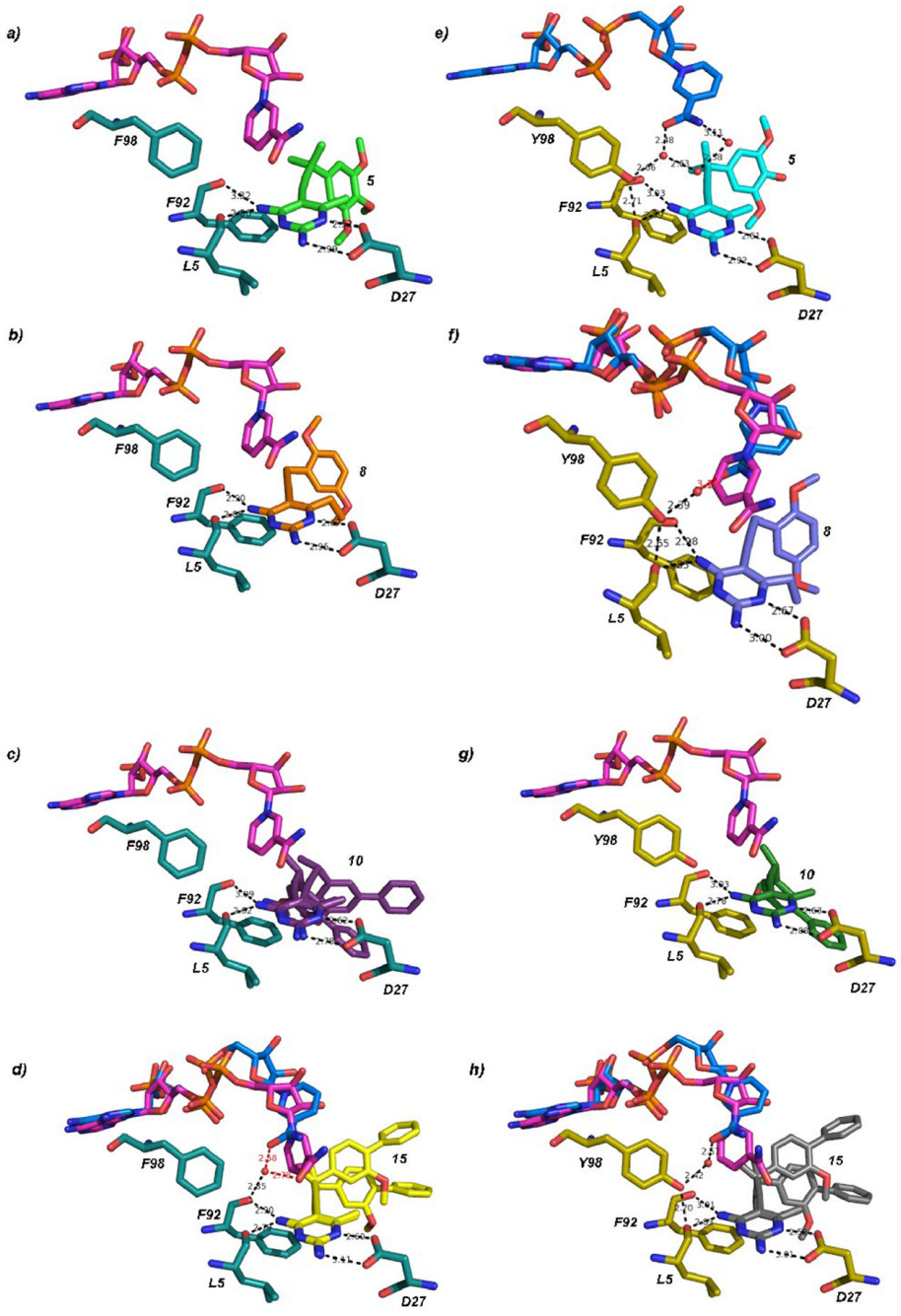

Figure 3.

Active site comparisons of a) SaDHFR:NADPH:**5**, b) SaDHFR:NADPH:**8**, c) SaDHFR:NADPH:**10**, d) SaDHFR:NADPH:**15**, e) Sa(F98Y)DHFR:NADPH:**5**, f) Sa(F98Y) DHFR:NADPH:**8**, g) Sa(F98Y)DHFR:NADPH:**10**, h) Sa(F98Y)DHFR:NADPH:**15**. The same coloring scheme is used as in Figure 1. Key water molecules are shown (red spheres), as are hydrogen bonds with distances labeled. Bond lengths are shown in black for full occupancy and red for less than full occupancy. In d, f, and h, two of the water molecules that are present for the alternative conformation are located at the same positions as the nicotinamide carbonyl and amino group and are not shown for clarity.

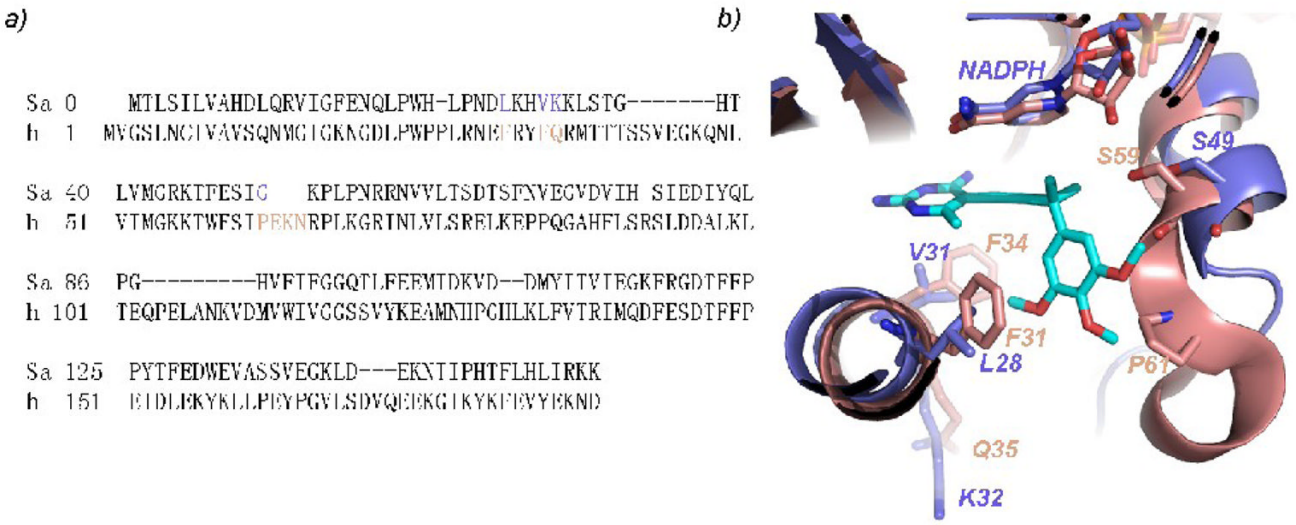

Figure 4.

a) Sequence alignment of SaDHFR and human DHFR and b) comparison of the structures of SaDHFR (purple) bound to compound **5** (cyan) and human DHFR (salmon) at the active site. Key residue differences are labeled.

Table 1

Potency and selectivity of DHFR inhibitors

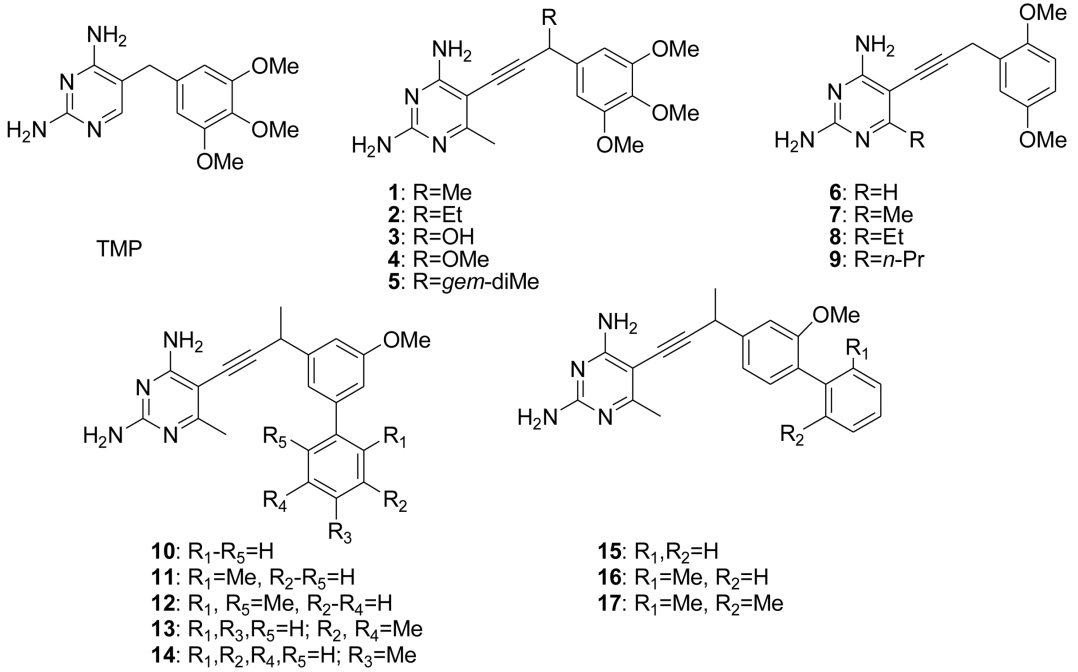

Compound	IC_{50} Sa WT (μM)	IC_{50} Sa (F98Y) (μM)	Potency Loss[a] (mut/wt)	IC_{50} human (μM)	Selectivity (h/Sa)[b]
TMP	0.023 ± 0.003	1.70 ± 0.02	73.9	198.2 ± 0.003	8608
1	0.17 ± 0.1	1.2 ± 0.009	7.1	1.38 ± 0.02	8.1
2	0.12 ± 0.05	3.9 ± 0.03	32.5	0.2 ± 0.01	1.7
3	1.1 ± 0.08	4.1 ± 0.03	3.7	5.7 ± 0.05	5.2
4	0.73 ± 0.01	12 ± 0.2	16.4	1.2 ± 0.007	1.6
5	0.064 ± 0.03	0.75 ± 0.07	11.7	0.29 ± 0.02	4.5
6	0.27 ± 0.1	6.9 ± 0.09	25.6	3.2 ± 0.05	11.8
7	0.27 ± 0.08	1.3 ± 0.007	4.8	1.3 ± 0.003	4.8
8	0.068 ± 0.006	0.67 ± 0.06	9.8	1.28 ± 0.02	18.8
9	0.048 ± 0.004	0.55 ± 0.04	11.4	1.18 ± 0.01	24.6

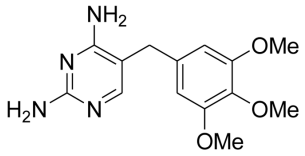

TMP

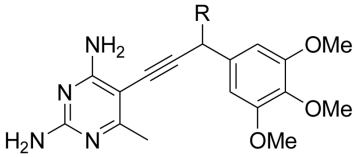

1: R=Me
2: R=Et
3: R=OH
4: R=OMe
5: R=*gem*-diMe

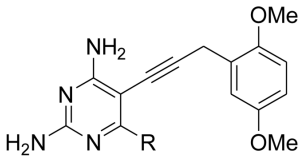

6: R=H
7: R=Me
8: R=Et
9: R=*n*-Pr

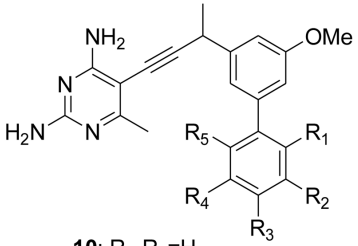

10: R_1-R_5=H
11: R_1=Me, R_2-R_5=H
12: R_1, R_5=Me, R_2-R_4=H
13: R_1,R_3,R_5=H; R_2, R_4=Me
14: R_1,R_2,R_4,R_5=H; R_3=Me

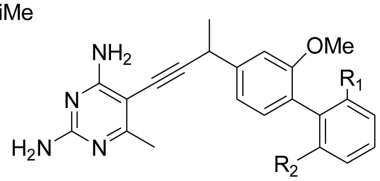

15: R_1,R_2=H
16: R_1=Me, R_2=H
17: R_1=Me, R_2=Me

Compound	IC_{50} Sa WT (μM)	IC_{50} Sa (F98Y) (μM)	Potency Loss[a] (mut/wt)	IC_{50} human (μM)	Selectivity (h/Sa)[b]
10	0.061 ± 0.03	0.19 ± 0.003	3.1	1.7 ± 0.01	27.9
11	0.073 ± 0.02	0.19 ± 0.07	2.6	1.4 ± 0.05	19.2
12	0.073 ± 0.02	0.18 ± 0.02	2.5	1.2 ± 0.006	16.4
13	0.042 ± 0.004	0.17 ± 0.02	4	0.75 ± 0.006	17.8
14	0.41 ± 0.04	0.96 ± 0.6	2.3	1.4 ± 0.02	3.4
15	0.17 ± 0.02	0.77 ± 0.06	4.5	1.4 ± 0.01	8.2
16	0.5 ± 0.06	1.42 ± 0.4	2.8	2.8 ± 0.06	5.6
17	0.41 ± 0.04	6.13 ± 0.5	15.8	3.4 ± 0.02	8.3

[a] Potency loss is calculated as the ratio of IC_{50} Sa(F98Y)/IC_{50} Sa

[b] Selectivity is calculated as the ratio of IC_{50} human/ IC_{50} Sa

Table 2

Data collection and refinement statistics for the eight reported structures

	Sa WT DHFR				**Sa(F98Y) DHFR**			
Ligand	**5**	**8**	**10**	**15**	**5**	**8**	**10**	**15**
PDB ID	**3FQC**	**3FQ0**	**3F0B**	**3FQZ**	**3FQF**	**3FQO**	**3F0U**	**3FQV**
Space Group	$P6_1$	$P6_122$	$P6_122$	$P6_122$	$P6_122$	$P6_122$	$P6_122$	$P6_122$
No. Molecules in Asymmetric Unit	2	1	1	1	1	1	1	1
Unit Cell (a,b,c in Å)	a=85.99, b=85.99, c=101.48	a=79.21, b=79.21, c=108.02	a=79.12, b=79.12, c=109.14	a=79.05, b=79.05, c=108.34	a=79.22, b=79.22, c=108.75	a=78.87, b=78.87, c=107.83	a=79.13, b=79.13, c=109.17	a=78.90, b=78.90, c=108.19
Resolution (Å)	42.99-2.35	31.94-1.69	25.4-2.10	31.94-1.72	32.72-1.77	42.33, 2.09	32.1-1.66	37.06-1.85
Last shell defined as (Å):	2.48-2.35	1.75-1.69	2.15-2.10	1.81-1.72	1.83-1.77	2.18-2.09	1.66-1.60	1.92-1.85
Completeness% (last shell, %)	99.6 (100)	97.9 (79.4)	95.8 (95.0)	99.5 (100)	89.4 (100)	99.1 (100)	96.5 (87.2)	99.2 (99.5)
Unique Reflections	16818	21315	11715	20665	17214	11686	22505	16599
Redundancy (last shell)	5.4 (5.2)	9.3 (3.7)	6.0 (4.1)	11.7 (11.1)	11.4 (11.1)	9.5 (9.4)	8.9 (1.5)	10.0 (8.1)
Rsym, % (last shell, %)	0.074 (0.387)	0.036 (0.245)	0.078 (0.288)	0.043 (0.306)	0.068 (0.167)	0.064 (0.406)	0.038 (0.212)	0.047 (0.096)
<I/σ> (last shell)	9.0 (5.3)	7.2 (2.2)	7.6 (3.3)	6.2 (4.9)	1.4 (1.1)	5.0 (3.8)	8.5 (2.5)	2.7 (0.9)
Refinement Statistics								
R_{cryst},R_{free}	0.204, 0.265	0.218, 0.250	0.203, 0.257	0.213, 0.242	0.209, 0.245	0.218, 0.261	0.212, 0.244	0.225, 0.266
No. of atoms (protein, ligands, solvent)	2546, 148, 144	1273, 71, 149	1273, 102, 132	1273, 150, 133	1274, 73, 193	1274, 119, 63	1274, 75, 161	1274, 150, 150
Rms deviation bond lengths (Å), angles (°)	0.009, 1.40	0.008, 1.28	0.011, 1.48	0.008, 1.46	0.008, 1.39	0.008, 1.42	0.010, 1.52	0.007, 1.42
Average B factor ($Å^2$)	47.2	22.3	30.7	15.2	14.9	30.6	23.4	18.2
Average B factor for ligand ($Å^2$)	40.6	19.4	18.1	12.7	10.3	26.6	24.2	14.3
Average B factor for solvent molecules ($Å^2$)	53.2	36.5	50.3	25.9	28.8	35.8	35.0	30.2
Ramachandran Plot Statistics								
Residues in most favored regions, allowed regions (%)	90.8, 9.2	90.4, 9.6	89.7, 10.3	91.2, 8.8	91.9, 8.1	91.9, 8.1	90.4, 9.6	91.9, 8.1

Table 3

Ligand and NADPH Occupancies and B-factors

	Sa WT DHFR				Sa(F98Y) DHFR			
Ligand	**Occup. Ligand (maj.,min.)**	**Occup. Std. NAP**	**Occup. Alt. NAP**	**B-factors (Ligand, NAP), Å^2**	**Occup. Ligand (maj.,min.)**	**Occup. Std. NAP**	**Occup. Alt. NAP**	**B-factors (Ligand, NAP), Å^2**
5	1.0	1.0	0	**A**[a]: 41.0 38.0 **B:** 40.2, 51.2	1.0	0	1.0	10.3,12.5
8	1.0	1.0	0	19.4 ,20.7	1.0	0.7	0.3	26.6 ,24.9
10	0.8, 0.2	1.0	0	24.2, 18.6	1.0	1.0	0	24.3, 18.6
15	0.6, 0.4	0.3	0.7	12.7, 11.7	0.6, 0.4	0.3	0.7	14.3, 16.5

[a]Chain A is denoted by **A**, chain B is denoted by **B**